

TWO-LAYER QUASI-GEOSTROPHIC MODEL — ATMOSPHERE AND OCEAN REGIMES

DI QI

In this report, we summarize the general formulation and instability of the two-layer quasi-geostrophic flow, and test the statistical features and the development of reduced-order methods through numerical simulations in both atmosphere and ocean regimes.

The potential vorticity equations for the **two-layer quasi-geostrophic flow with topography** can be written as

$$(0.1) \quad \frac{\partial q_i}{\partial t} + J(\psi_i, q_i) + \beta \frac{\partial \psi_i}{\partial x} + U_i \frac{\partial}{\partial x} \nabla^2 \psi_i + \frac{k_d^2}{2} \left(U_i \frac{\partial \psi_{3-i}}{\partial x} - U_{3-i} \frac{\partial \psi_i}{\partial x} \right) = -\delta_{i2} \left(U_i \frac{\partial h}{\partial x} + \kappa \nabla^2 \psi_i \right), \quad i = 1, 2.$$

Above the potential vorticity disturbance in the upper layer ($i = 1$) and lower layer ($i = 2$) is defined as

$$(0.2) \quad q_1 = \nabla^2 \psi_1 + \frac{k_d^2}{2} (\psi_2 - \psi_1), \quad q_2 = \nabla^2 \psi_2 + \frac{k_d^2}{2} (\psi_1 - \psi_2) + h.$$

Topographic structure h is introduced into the system in the additional term in the lower layer potential vorticity. (U_1, U_2) is the mean flow in the upper and lower layer, and usually we assume the flow follows in the form

$$(0.3) \quad U_1 = U_0 + U, \quad U_2 = U_0 - U,$$

where U_0 is the mean structure and U is the shear between the two layers. The system will reduce to the barotropic flow when $U = 0$. Besides in (0.1), $J(A, B) = A_x B_y - A_y B_x$ represents the Jacobian operator. $k_d = \sqrt{8}/L_d = (2f_0/NH)^2$ is the baroclinic deformation wavenumber corresponding to the Rossby radius of deformation L_d . For simplicity we will always consider the case with equal layer depth model, $H_1 = H_2 = H/2$ (which might not be a feasible and realistic assumption especially in the ocean regime, but several complicated additional terms will be avoided in the equal-depth case thus it is a desirable test case).

Besides, considering the conservation of energy including the topography, we can also introduce **the dynamics for the large-scale mean flow**

$$\frac{dU_0}{dt} = \oint \psi_2 \frac{\partial h}{\partial x}, \quad \frac{dU}{dt} = -\oint \psi_2 \frac{\partial h}{\partial x}.$$

The large-scale energy becomes $\frac{1}{2} (U_0^2 + U^2)$.

1. FLUCTUATION EQUATIONS OF THE TWO-LAYER QG EQUATIONS AND CONSERVED QUANTITIES WITHOUT FORCING AND DISSIPATION

1.1. Linear relation between the streamfunction and potential vorticity. Following the same procedure of the one-layer barotropic flow, we consider to develop the fluctuation equations of the two-layer QG equations about the assumed mean state. If we define **the total stream functions Ψ_1 in the upper layer, and Ψ_2 in the lower layer** as

$$(1.1) \quad \Psi_1 = -U_1 y + \psi_1, \quad \Psi_2 = -U_2 y + \psi_2.$$

We assume a uniform background large-scale shear with strength (U_1, U_2) in the upper and lower layers, and (ψ_1, ψ_2) are the perturbed stream functions in the upper and lower layers. Accordingly, we can define the total potential vorticities (Q_1, Q_2) in the upper and lower layer as

$$(1.2) \quad Q_i = \bar{Q}_i + q_i = \bar{Q}_i + \Delta \psi_i + \frac{k_d^2}{2} (\psi_{3-i} - \psi_i), \quad i = 1, 2,$$

$$\bar{Q}_i(y) = \beta y - \frac{k_d^2}{2} (U_{3-i} - U_i) y, \quad q_i = \Delta \psi_i + \frac{k_d^2}{2} (\psi_{3-i} - \psi_i) + \delta_{2i} h, \quad i = 1, 2.$$

Again we decompose the entire potential vorticity Q_i into the large-scale basic flow, \bar{Q}_i , and the disturbance, q_i . We assume the simple linear relation between the mean streamfunction and potential vorticity in both small and large scales and in both upper and lower layers

$$(1.3) \quad \begin{aligned} \mu_1 \bar{\Psi}_1 &= \bar{Q}_1, \quad \mu_1 \bar{\psi}_1 = \bar{q}_1 = \nabla^2 \bar{\psi}_1 + \frac{k_d^2}{2} (\bar{\psi}_2 - \bar{\psi}_1), \\ \mu_2 \bar{\Psi}_2 &= \bar{Q}_2, \quad \mu_2 \bar{\psi}_2 = \bar{q}_2 = \nabla^2 \bar{\psi}_2 + \frac{k_d^2}{2} (\bar{\psi}_1 - \bar{\psi}_2) + h. \end{aligned}$$

From the large-scale relations between \bar{Q}_i and $\bar{\Psi}_i$, we can get the parameter values using the fact $U_1 - U_2 = 2U$ so that

$$(1.4) \quad \begin{aligned} \mu_1 &= -(\beta + k_d^2 U) / (U_0 + U), \\ \mu_2 &= -(\beta - k_d^2 U) / (U_0 - U). \end{aligned}$$

Then consider the small-scale solution following the linear relations in (1.3). The solution comes from the linear system

$$\begin{pmatrix} \mu_2 + |\mathbf{k}|^2 + \frac{k_d^2}{2} & -\frac{k_d^2}{2} \\ -\frac{k_d^2}{2} & \mu_2 + |\mathbf{k}|^2 + \frac{k_d^2}{2} \end{pmatrix} \begin{pmatrix} \bar{\psi}_{1,\mathbf{k}} \\ \bar{\psi}_{2,\mathbf{k}} \end{pmatrix} = \begin{pmatrix} 0 \\ \hat{h}_{\mathbf{k}} \end{pmatrix}.$$

Therefore the small-scale mean state can be solved as

$$(1.5) \quad \begin{aligned} \bar{\psi}_{1,\mathbf{k}} &= \frac{A^{-1}}{2} k_d^2 \hat{h}_{\mathbf{k}}, \\ \bar{\psi}_{2,\mathbf{k}} &= A^{-1} \left(\mu_2 + |\mathbf{k}|^2 + \frac{k_d^2}{2} \right) \hat{h}_{\mathbf{k}}, \end{aligned}$$

where

$$A = \left(|\mathbf{k}|^2 + \mu_1 \right) \left(|\mathbf{k}|^2 + \mu_2 \right) + k_d^2 \left(|\mathbf{k}|^2 + \frac{1}{2} (\mu_1 + \mu_2) \right),$$

is the determinant of the coefficient matrix. The mean state solution will explode near the resonant wavenumber where the determinant is zero, $A = 0$. And for other wavenumbers the mean state solution will be determined uniquely by (1.5).

Here we have a little more discussion about the case with no averaged flow $U_0 = 0$, and no topography $h \equiv 0$. Especially, when the topography is zero, $\hat{h}_{\mathbf{k}} \equiv 0$, the allowed mean state is zero at most of the wavenumbers

$$(1.6) \quad \bar{\psi}_{1,\mathbf{k}} = \bar{\psi}_{2,\mathbf{k}} \equiv 0,$$

except for the selected resonant modes where the determinant reaches zero $A = 0$. This implies the homogeneous solution in the unforced two-layer equations in statistical steady state, and we need only focus on the second order moments in the statistical formulations. Again consider the special case $U_0 = 0$, the linear relation parameters (1.4) become

$$(1.7) \quad \begin{aligned} \mu_1 &= -k_{\beta}^2 - k_d^2, \\ \mu_2 &= k_{\beta}^2 - k_d^2, \end{aligned}$$

with $k_{\beta}^2 = \beta/U$ the wavenumber related with the β -effect. Note that in this case, μ_1 is always negative, while the sign of μ_2 is not determined depending on the amplitudes of k_{β} and k_d . The possible non-zero (resonant) modes can only happen at wavenumbers with zero determinant

$$A = |\mathbf{k}|^2 \left(|\mathbf{k}|^2 - k_d^2 \right) - k_{\beta}^4 \Rightarrow |\mathbf{k}|^2 = \frac{1}{2} \left[k_d^2 + (k_d^4 + 4k_{\beta}^4)^{1/2} \right].$$

Therefore the resonant regime where the mean state can take non-zero values can only take place among the regimes

$$k_d < |\mathbf{k}| < \sqrt{k_d^2 + k_{\beta}^2}.$$

1.2. Fluctuation equations of the two-layer equations. Following the linear relationship between the streamfunction and relative vorticity (1.3), we can derive the fluctuation equations about the mean state using the same set of strategies as in the barotropic flow. Again we assume the small-scale streamfunctions can be decomposed into the statistical mean and fluctuations about the mean state

$$\psi_1 = \bar{\psi}_1 + \psi'_1, \quad \psi_2 = \bar{\psi}_2 + \psi'_2.$$

For the nonlinear interaction part in the original equations (0.1), the mean state $\bar{\psi}_i$ will interact with the combined quantity $q'_i - \mu_i \psi'_i$. In the linear part, due to the parameter values determined in (1.4) the terms related with the mean state will all cancel out. To summarize, the **fluctuation equations about the mean state without considering forcing and dissipation** can be formulated as

$$(1.8) \quad \frac{\partial q'_1}{\partial t} + \nabla^\perp \bar{\psi}_1 \cdot \nabla (q'_1 - \mu_1 \psi'_1) + \nabla^\perp \psi'_1 \cdot \nabla q'_1 = -U_1 \frac{\partial q'_1}{\partial x} - (\beta + k_d^2 U) \frac{\partial \psi'_1}{\partial x},$$

$$(1.9) \quad \frac{\partial q'_2}{\partial t} + \nabla^\perp \bar{\psi}_2 \cdot \nabla (q'_2 - \mu_2 \psi'_2) + \nabla^\perp \psi'_2 \cdot \nabla q'_2 = -U_2 \frac{\partial q'_2}{\partial x} - (\beta - k_d^2 U) \frac{\partial \psi'_2}{\partial x}.$$

Note that the mean-fluctuation interactions are only introduced through the additional term, $\nabla^\perp \bar{\psi}_i \cdot \nabla (q'_i - \mu_i \psi'_i)$, while all the other terms stay the same with the original two-layer system (0.1). The fluctuation equations describe the evolution about the fluctuating part around the mean state in the two-layer flow and offer the convenience to focus on the variances in each spectral mode. For simplicity we will drop the ‘prime’ for the fluctuating components in the above formulations.

1.3. Conserved quantities in the two-layer equations. In this final part of this section, we discuss the conserved quantities in the fluctuation equations (1.8)-(1.9). (Note that since the nonlinear quadratic part conserves both energy and enstrophy, the results can also apply to the original two-layer flow in (0.1).) First following exactly the same reasoning for the barotropic flow, we can first find out that the nonlinear interaction part, $\nabla^\perp \psi'_i \cdot \nabla q'_i$, conserves both energy and enstrophy. On the other hand, due to the baroclinic instability in the two-layer flow, additional terms representing meridional heat transfer will take place in both energy and enstrophy equations. Consider the energy and (scaled) enstrophy defined as

$$E = \frac{1}{2} \int | \nabla \psi_1 |^2 + | \nabla \psi_2 |^2 + \frac{k_d^2}{2} (\psi_1 - \psi_2)^2 = \int | \nabla \psi |^2 + | \nabla \tau |^2 + k_d^2 \tau^2,$$

$$\tilde{\mathcal{E}}(\mu_1, \mu_2) = \frac{1}{2} \int \mu_1^{-1} | q_1 |^2 + \mu_2^{-1} | q_2 |^2.$$

Through the dynamics (1.8)-(1.9) and the parameter values from (1.4), we can find the equation

$$\begin{aligned} \frac{dE}{dt} &= -\frac{k_d^2}{2} U \int \psi_2 \frac{\partial \psi_1}{\partial x} - \psi_1 \frac{\partial \psi_2}{\partial x} = 0, \\ \frac{d\tilde{\mathcal{E}}}{dt} &+ \frac{k_d^2}{2} U \int \psi_2 \frac{\partial \psi_1}{\partial x} - \psi_1 \frac{\partial \psi_2}{\partial x} \end{aligned}$$

Note that the middle line above usually represents the meridional heat flux, $k_d^2 U f v \tau$. Therefore we find the conserved quantity $\tilde{\mathcal{E}} + E$ so that

$$(1.10) \quad \frac{d}{dt} (\tilde{\mathcal{E}} + E) = 0,$$

where

$$(1.11) \quad \tilde{\mathcal{E}} + E = \frac{1}{2} \int | \nabla \psi_1 |^2 + | \nabla \psi_2 |^2 + \frac{k_d^2}{2} (\psi_1 - \psi_2)^2 + \mu_1^{-1} | q_1 |^2 + \mu_2^{-1} | q_2 |^2.$$

Note that again in the case $U_0 = 0$, and $\mu_1 = -k_\beta^2 - k_d^2$, $\mu_2 = k_\beta^2 - k_d^2$. The quantity is not positive-definite, stability features cannot be derived from this conservation quantity.

1.4. Conservation in the homogeneous case $\bar{\psi}_i \equiv 0$. Now we consider the special homogeneous case, $\bar{\psi}_i = 0$. Then the fluctuation equations (1.8)-(1.9) become the same with the original two-layer equations (0.1), while still the above conserved quantity is valid for $\tilde{\mathcal{E}} + E$. Consider the original enstrophy

$$\mathcal{E} = \frac{1}{2} \oint |q_1|^2 + |q_2|^2 = \oint |q_\psi|^2 + |q_\tau|^2.$$

Applying similar analysis as before we can find another conserved quantity for the two-layer system

$$(1.12) \quad \frac{d}{dt} (-k_d^{-2} \mathcal{E} + E) = 0,$$

where

$$(1.13) \quad -k_d^2 \mathcal{E} + E = \frac{1}{2} \oint |\nabla \psi_1|^2 + |\nabla \psi_2|^2 + \frac{k_d^2}{2} (\psi_1 - \psi_2)^2 - k_d^{-2} (|q_1|^2 + |q_2|^2).$$

Again this is not a positive-definite quantity. Yet by combining the two conserved quantities from (1.11) and (1.13) we can find the new conserved quantity

$$(1.14) \quad \tilde{\mathcal{E}} + k_d^2 \mathcal{E} = (k_d^{-2} + \mu_1^{-1}) |q_1|^2 + (k_d^{-2} + \mu_2^{-1}) |q_2|^2.$$

Consider the case $U_0 = 0$, and $\mu_1 = -k_\beta^2 - k_d^2$, $\mu_2 = k_\beta^2 - k_d^2$, we can derive the relation

$$\begin{aligned} & (k_\beta^2 - k_d^2) |q_1|^2 + (k_\beta^2 + k_d^2) |q_2|^2. \\ & |q_1|^2 = \sum |k^2 \psi_k + (k^2 + k_d^2) \tau_k|^2, \\ & |q_2|^2 = \sum |k^2 \psi_k - (k^2 + k_d^2) \tau_k|^2. \end{aligned}$$

If $k_\beta > k_d$, the above conserved quantity is positive-definite, thus the system is nonlinearly stable for the entire process in the sense that the variance in the fluctuations can be controlled by the initial uncertainty (and this is also consistent with the results from linear analysis); if $k_\beta \leq k_d$, we may find the ratio for the exchange of enstrophy between the upper and lower layer as,

$$\delta |q_1|^2 = \frac{k_d^2 + k_\beta^2}{k_d^2 - k_\beta^2} \delta |q_2|^2.$$

This relation characterizes the sensitivity of the enstrophy in the upper layer if the enstrophy in the lower layer is damped or forced. In the limit $k_d \gg k_\beta$, the variance fluctuations in the upper and lower layer can layer in relatively the same amplitude, $\delta |q_1|^2 \sim \delta |q_2|^2$; on the other hand, when $k_d \gtrsim k_\beta$ with comparable amplitude, the changes in the variance fluctuation in the lower layer $\delta |q_2|^2$ can lead to large changes in the upper layer $\delta |q_1|^2$.

2. FORMULATION OF THE TWO-LAYER QG MODEL IN BAROTROPIC AND BAROCLINIC COMPONENT

We consider the *Phillips model* in a barotropic-baroclinic mode formulation for potential vorticity anomalies (q_ψ, q_τ) with periodic boundary condition in both x, y directions

$$(2.1) \quad \begin{aligned} \frac{\partial q_\psi}{\partial t} + J(\psi, q_\psi) + J(\tau, q_\tau) + \beta \frac{\partial \psi}{\partial x} + U \frac{\partial}{\partial x} \Delta \tau + U_0 \frac{\partial q_\psi}{\partial x} &= -\frac{\kappa}{2} \Delta(\psi - \tau) - \nu \Delta^s q_\psi + \mathcal{F}_\psi(\mathbf{x}, t), \\ \frac{\partial q_\tau}{\partial t} + J(\psi, q_\tau) + J(\tau, q_\psi) + \beta \frac{\partial \tau}{\partial x} + U \frac{\partial}{\partial x} (\Delta \psi + k_d^2 \psi) + U_0 \frac{\partial q_\tau}{\partial x} &= \frac{\kappa}{2} \Delta(\psi - \tau) - \nu \Delta^s q_\tau + \mathcal{F}_\tau(\mathbf{x}, t). \end{aligned}$$

Here $q_\psi = \Delta \psi$, $q_\tau = \Delta \tau - k_d^2 \tau$ are the perturbed potential vorticity in barotropic and baroclinic mode respectively, while ψ, τ are the corresponding perturbed barotropic and baroclinic stream functions. k_d is the wavenumber corresponding to the Rossby radius of deformation. Here the flow is assumed with periodic geometry in the horizontal directions, and with a flat bottom, rigid lid $h = 0$ in the two vertical layers denoted as q_1 (upper layer) and q_2 (lower layer) in subscripts. The relations between the upper and lower layer relative vorticity and stream function with the barotropic and baroclinic modes can be defined through the following relations

$$\begin{aligned} q_\psi &= \nabla^2 \psi = \frac{1}{2} (q_1 + q_2), & \psi &= \frac{1}{2} (\psi_1 + \psi_2), \\ q_\tau &= \nabla^2 \tau - k_d^2 \tau = \frac{1}{2} (q_1 - q_2), & \tau &= \frac{1}{2} (\psi_1 - \psi_2). \end{aligned}$$

The barotropic mode ψ can be viewed as the vertically averaged effect from the flow, and the baroclinic mode τ is usually related with the thermal effect in heat transport. Note the additional terms due to the mean large-scale flow U_0 for both barotropic and baroclinic modes. For simplicity we will always assume $U_0 = 0$ for the rest of the discussions.

On the right hand side of the equation (2.1), first we assume the dissipation is only from the Ekman damping together with the hyperviscosity terms $\nu\Delta^s$, with s chosen as a even integer depending on the resolution of the model such that it only damps the smaller scales. That is, in the dynamical equations of the two-layer form (q_1, q_2) , it is equivalent to a linear damping on the lower layer mode, $-\kappa\nabla^2\psi_2$, and no dissipation terms on the upper layer, q_1 . For the forcing terms $\mathcal{F}_\psi, \mathcal{F}_\tau$, it is decomposed into the deterministic part, and random component represented by Gaussian white noises

$$(2.2) \quad \begin{aligned} \mathcal{F}_\psi(\mathbf{x}, t) &= f_\psi(\mathbf{x}, t) + \sigma_\psi(\mathbf{x}) \dot{W}_\psi(t), \\ \mathcal{F}_\tau(\mathbf{x}, t) &= f_\tau(\mathbf{x}, t) + \sigma_\tau(\mathbf{x}) \dot{W}_\tau(t). \end{aligned}$$

Examples of the large-scale forcing terms can include radiative heating, surface wind stress etc., while convective storms, unresolved baroclinic instability process can act as the forcing on small length scales. Usually the two-layer system will reach an equilibrium statistical steady state without any forcing perturbations, and it is interesting research topic to investigate the system's responses according to the external forcing perturbations due to various effects from nature. In the barotropic and baroclinic dynamical equations, the nonlinear interaction in the barotropic dynamics includes the quadratic forms in the barotropic and baroclinic mode independently, while the nonlinear interaction in the baroclinic dynamics are the quadratic forms between barotropic and baroclinic modes as well as a term due to the non-equal layers.

2.1. Symmetries in the nonlinear quadratic forms and normalized equations. In model simulations and developing reduced models, it is useful to introduce a new set of rescaled quantities

$$(2.3) \quad \begin{aligned} p_{\psi,\mathbf{k}} &= q_{\psi,\mathbf{k}} / |\mathbf{k}| = -|\mathbf{k}| \psi_\mathbf{k}, \\ p_{\tau,\mathbf{k}} &= q_{\tau,\mathbf{k}} / \sqrt{|\mathbf{k}| + k_d^2} = -\sqrt{|\mathbf{k}| + k_d^2} \psi_\mathbf{k}. \end{aligned}$$

The benefits by introducing this new set of quantities (2.3) include: i) the energy inner-product reduces to the standard Euclidean form; ii) p_ψ, p_τ share the same value of amplitude especially for the ocean regime when k_d becomes large. Under the above setting-ups, the rescaled set of equations of (2.1) become

$$(2.4) \quad \frac{d\mathbf{p}_\mathbf{k}}{dt} = B_\mathbf{k}(\mathbf{p}_\mathbf{k}, \mathbf{p}_\mathbf{k}) + (\mathcal{L}_\mathbf{k} - \mathcal{D}_\mathbf{k}) \mathbf{p}_\mathbf{k} + \mathcal{F}_\mathbf{k}, \quad \mathbf{p}_\mathbf{k} = (p_{\psi,\mathbf{k}}, p_{\tau,\mathbf{k}})^T,$$

where the nonlinear interactions become

$$B_\mathbf{k}(\mathbf{p}_\mathbf{k}, \mathbf{p}_\mathbf{k}) = \begin{pmatrix} \sum_{\mathbf{m}+\mathbf{n}=\mathbf{k}} \mathbf{m}^\perp \cdot \mathbf{n} \left(\frac{|\mathbf{n}|}{|\mathbf{m}|} p_{\psi,\mathbf{m}} p_{\psi,\mathbf{n}} + \sqrt{\frac{|\mathbf{n}|^2 + k_d^2}{|\mathbf{m}|^2 + k_d^2}} p_{\tau,\mathbf{m}} p_{\tau,\mathbf{n}} \right) \\ \sum_{\mathbf{m}+\mathbf{n}=\mathbf{k}} \mathbf{m}^\perp \cdot \mathbf{n} \left(\frac{\sqrt{|\mathbf{n}|^2 + k_d^2}}{|\mathbf{m}|} p_{\psi,\mathbf{m}} p_{\tau,\mathbf{n}} + \frac{|\mathbf{n}|}{\sqrt{|\mathbf{m}|^2 + k_d^2}} p_{\tau,\mathbf{m}} p_{\psi,\mathbf{n}} \right) \end{pmatrix},$$

and the linear operators are decomposed into the skew-symmetric part and dissipation part, together with the forcing terms in deterministic component and stochastic component

$$\mathcal{L}_\mathbf{k} = \begin{bmatrix} \frac{ik_x\beta}{|\mathbf{k}|^2} & -\frac{ik_x U}{\sqrt{1+(k_d/|\mathbf{k}|)^2}} \\ -ik_x U \frac{1-(k_d/|\mathbf{k}|)^2}{\sqrt{1+(k_d/|\mathbf{k}|)^2}} & \frac{ik_x\beta}{|\mathbf{k}|^2+k_d^2} \end{bmatrix}, \quad \mathcal{D}_\mathbf{k} = \frac{\kappa}{2} \begin{bmatrix} -1 & \frac{1}{\sqrt{1+(k_d/|\mathbf{k}|)^2}} \\ \frac{1}{\sqrt{1+(k_d/|\mathbf{k}|)^2}} & -\frac{1}{1+(k_d/|\mathbf{k}|)^2} \end{bmatrix}, \quad \mathcal{F}_\mathbf{k} = \begin{bmatrix} \frac{f_{\psi,\mathbf{k}}}{|\mathbf{k}|} + \frac{\sigma_{\psi,\mathbf{k}} \dot{W}_{\psi,\mathbf{k}}}{|\mathbf{k}|} \\ \frac{f_{\tau,\mathbf{k}}}{\sqrt{|\mathbf{k}|^2+k_d^2}} + \frac{\sigma_{\tau,\mathbf{k}} \dot{W}_{\tau,\mathbf{k}}}{\sqrt{|\mathbf{k}|^2+k_d^2}} \end{bmatrix}.$$

From the above equation (2.4), the first and second order moment dynamics are only coupled through the quadratic nonlinear interactions, $B(\mathbf{p}, \mathbf{p})$. In the development of reduced order models, this is the most expensive but crucial part to estimate. Therefore a careful calibration about this nonlinear interaction terms becomes the central role in the designing of the low-order methods as discussed in the following section.

2.2. Equilibrium unperturbed statistics in ocean and atmosphere regime.

parameter	ocean		atmosphere	
	dimensional	non-dimensional	dimensional	non-dimensional
L	200 km	-	1000 km	-
T	93 days (8×10^6 s)	-	1.93 days (1.67×10^5 s)	-
U_0	0.025 ms^{-1}	-	6 ms^{-1}	-
domain size $2\pi L$	1257 km	$k = 1$	6283 km	$k = 1$
Deformation radius λ	126 km	$k_d = 10$	1571 km	$k_d = 4$
β -effect	$6.25 \times 10^{-12} \text{ m}^{-1} \text{ s}^{-1}$	$\beta = 10$	$8.889 \times 10^{-12} \text{ m}^{-1} \text{ s}^{-1}$	$\beta = 1$
latitude θ	74°	-	75°	-
mean flow U	0.025 ms^{-1}	$U = 1$	1.2 ms^{-1}	$U = 0.2$
friction decay time τ_κ	10 days	$\kappa = 9$	9.65 days	$\kappa = 0.2$
time step Δt	1.1 hours (4000 s)	$\Delta t = 5 \times 10^{-4}$	13.9 mins (375 s)	$\Delta t = 5 \times 10^{-3}$
total run time	44 years	$N = 3.5 \times 10^5$	9.25 years	$N = 3.5 \times 10^5$

TABLE 1. Reference parameters in oceanic and atmospheric domain.

2.2.1. *Dimension analysis for the equations.* To relate the non-dimensionalized equations (2.1) with the realistic physical values in the oceanic and atmospheric domains, we carry out the simple dimensional analysis for the model parameters. Supposing the real domain size $2\pi L$ and the characteristic mean flow field $U_0 = L/T$ with T the characteristic time scale, we can find the scaling between dimensional and non-dimensional variables

$$\tilde{x} = Lx, \quad \tilde{t} = Tt, \quad q_\psi = \nabla^2 \psi = L^2 \tilde{\nabla}^2 \tilde{\psi}, \quad q_\tau = (\nabla^2 - k_d^2) \tau = (L^2 \tilde{\nabla}^2 - k_d^2) \tilde{\tau},$$

where the tilded variables $(\tilde{x}, \tilde{t}, \tilde{\psi}, \tilde{\tau})$ are the *dimensional ones* with physical units and the variables (x, t, ψ, τ) are the *scaled non-dimensional ones*. Therefore we can recover the dimensional equations about the variables of interests from the original non-dimensionalized equations (2.1) as

$$\begin{aligned} & \frac{\partial}{\partial \tilde{t}} \tilde{\nabla}^2 \tilde{\psi} + \beta L^{-1} T^{-1} \frac{\partial \tilde{\psi}}{\partial \tilde{x}} + U L T^{-1} \frac{\partial}{\partial \tilde{x}} \tilde{\Delta} \tilde{\tau} \\ &= -\frac{\kappa}{2} T^{-1} \tilde{\Delta} (\tilde{\psi} - \tilde{\tau}) - \nu L^{2s} T^{-1} \tilde{\Delta}^{s+1} \tilde{\psi} + U_0 L^{-1} T^{-1} \mathcal{F}_\psi, \\ & \frac{\partial}{\partial \tilde{t}} (\tilde{\nabla}^2 - k_d^2 L^{-2}) \tilde{\tau} + \beta L^{-1} T^{-1} \frac{\partial \tilde{\tau}}{\partial \tilde{x}} + U L T^{-1} \frac{\partial}{\partial \tilde{x}} (\tilde{\Delta} \tilde{\psi} + k_d^2 L^{-2} \tilde{\psi}) \\ &= \frac{\kappa}{2} T^{-1} \tilde{\Delta} (\tilde{\psi} - \tilde{\tau}) - \nu L^{2s} T^{-1} \Delta^s (\tilde{\nabla}^2 - k_d^2 L^{-2}) \tilde{\tau} + U_0 L^{-1} T^{-1} \mathcal{F}_\tau. \end{aligned}$$

Comparing the above dimensional equations with the original non-dimensionalized system, the scales in the parameters can be realized as

$$(2.5) \quad \tilde{\lambda} = L\lambda, \quad \tilde{\beta} = \frac{U_0}{L^2} \beta, \quad \tilde{U} = U_0 U, \quad \tilde{\tau}_\kappa = T \tau_\kappa, \quad \tilde{\mathcal{F}} = U_0^2 L^{-2} \mathcal{F}.$$

where $\lambda = k_d^{-1}$ is the (first) deformation radius, $\tau_\kappa = \kappa^{-1}$ is the Ekman friction decay time, and note U is the (scaled) large-scale mean flow field while U_0 is characteristic flow velocity.

With the understanding about the physical parameters in (2.5), we propose the reference parameters for the oceanic and atmospheric domain as in Table 1. The parameters are chosen to obtain nonlinear interaction and response. In the oceanic regime, with a domain size of about 2500 km and a velocity unit of 0.05 ms^{-1} , the time unit $T = L/U$ is of the order of 100 days. In the atmospheric regime, we find a larger domain size near 10000 km and faster critical velocity field $U = 20 \text{ ms}^{-1}$. Note that the ocean regime becomes a stiff problem and much smaller time step should be chosen to make sure the scheme is stable. We integrate the system to an extremely long time $N = 3.5 \times 10^5$ in order to get relatively accurate statistical results.

2.2.2. *Homogeneous statistics in equilibrium.* Here we check the performance of the two-layer quasi-geostrophic flow (2.1) in high-latitude ocean and atmosphere regime through direct numerical simulations. We apply the pseudo-spectral method to the barotropic flow to get the simulation results. For the nonlinear advection term, $\mathcal{P}_\Lambda (\nabla^\perp \psi_\Lambda \cdot \nabla q_\Lambda)$, the standard 3/2-rule is applied to avoid aliasing error. In all the following simulations, we choose the high wavenumber truncation as, $\Lambda = 256$. For the time integration, we use the standard 4-th order Runge-Kutta methods with time step $\Delta t = 5 \times 10^{-4}$ and $\Delta t = 5 \times 10^{-3}$ for ocean ant atmosphere regime respectively,

regime	N	β	k_d	U	κ	ν	s
ocean regime, high lat.	256	10	10	1	9	1.2×10^{-15}	4
atmosphere regime, high lat.	256	1	4	0.2	0.2	5×10^{-15}	4

TABLE 2. Model parameters for ocean and atmosphere dynamical regimes in high latitude. N is the model resolution, β , k_d are the rotation parameter and the deformation frequency, U is the background mean flow, κ is the Ekman drag in the bottom layer, and the hyperviscosity is measured by the operator $-\nu \nabla^2 s$.

which is small enough to capture all the small-scale dynamics. The time-series are recorded at every 20 or 10 time steps, that is, we sample the data at every 0.01 or 0.05 time unit. We integrate the system up to a long time with $N = 3.5 \times 10^5$ time steps with the first 2000 steps skipped in the calculation of model statistics. Small hyperviscosity, $\nu = 1.2 \times 10^{-15}$, is added to both barotropic and baroclinic modes to dissipate the unresolved small-scale fluctuations. In all the simulation cases for the unperturbed system, no external forcing is added in neither deterministic nor stochastic component. Parameters for three different dynamical regimes are shown in Table 2. The two sets of parameters correspond to the high and low latitude ocean regimes. The parameters are chosen so that baroclinic instability is exhibited in a wide range of modes $\frac{\beta}{2U} \leq |\mathbf{k}| \leq k_d$ with a turbulent cascade.

Figure 2.1 displays the equilibrium statistics for the two-layer flow in high-latitude ocean regime. The first row shows the snapshots of the barotropic and baroclinic modes. Homogeneous structure can be observed in both cases. It is important to notice the strong correlation in the coherent structures in the barotropic and baroclinic field, illustrating the strong energy transfer (heat flux) between the two modes.

In Figure 2.2 the results for the two-layer flow in high-latitude atmosphere regime are compared. In this atmosphere regime one important feature is that the flow is alternating between the blocked and unblocked regimes. Typical snapshots for the blocked and unblocked regime are shown. In the blocked regime, strong poleward heat transfer appears due to the baroclinic instability, while in the unblocked regime the flow appears more zonal with jet structures in x -direction. Following we plot the time-series for the evolvement of barotropic and baroclinic energy together with the heat flux $f \frac{\partial \psi}{\partial x} \tau$ which illustrates the meridional heat transfer. First note that the peaks in the baroclinic energy is always accompanied with strong poleward heat transfer. This is due to the baroclinic instability in the flow. Second, note that the peaks in the barotropic energy is always behind the baroclinic peaks, which is due to the nonlinear interactions between the barotropic and baroclinic modes (this also implies that in the reduced-order methods, injecting energy in the barotropic modes is easier than in the baroclinic modes since weaker nonlinear interactions will be involved).

The radial averaged spectra for the mean and variance (energy) in each mode are followed in the figure. In the intermediate inertia range, both the barotropic and baroclinic mode spectra display a decay rate about $\sim k^{-2}$ in the ocean case and a rate about $\sim k^{-1.6}$ in the atmosphere case.. The homogeneous statistical structure is further guaranteed by the small amplitude of the mean field in both ocean and atmosphere regimes (within the range of numerical fluctuations).

3. STABILITY ANALYSIS IN THE TWO-LAYER SYSTEM

Here we investigate the instability in the two-layer model and consider the nonlinear energy transfer through the nonlinear flux. We compare the results from the linear analysis for linear growth rates and the instability from the nonlinear flux.

3.1. Linear instability analysis. We analyze the linear stability for the two-layer QG model (2.1) with generality to unequal layers, using $\delta = H_1/H$ the ratio of the upper layer to total depth, and $\xi = (1 - 2\delta)/\sqrt{\delta(1 - \delta)}$. Following the general procedure like in Vallis or Pedlosky, we can consider the stream functions of single mode with zonal phase velocity,

$$\psi = \hat{\psi}_{\mathbf{k}} e^{i\mathbf{k} \cdot \mathbf{x}} e^{-ik_1 ct}, \quad \tau = \hat{\tau}_{\mathbf{k}} e^{i\mathbf{k} \cdot \mathbf{x}} e^{-ik_1 ct}.$$

Thus the stability of the stream functions ψ, τ can be decided by the imaginary part of the phase velocity, c . Correspondingly, we can get the potential vorticity of single mode, $q_{\psi} = \hat{q}_{\psi, \mathbf{k}} e^{i\mathbf{k} \cdot \mathbf{x}} e^{-ik_1 ct}$, $q_{\tau} = \hat{q}_{\tau, \mathbf{k}} e^{i\mathbf{k} \cdot \mathbf{x}} e^{-ik_1 ct}$, as

$$\hat{q}_{\psi, \mathbf{k}} = -|\mathbf{k}|^2 \hat{\psi}_{\mathbf{k}}, \quad \hat{q}_{\tau, \mathbf{k}} = -(|\mathbf{k}|^2 + k_d^2) \hat{\tau}_{\mathbf{k}}.$$

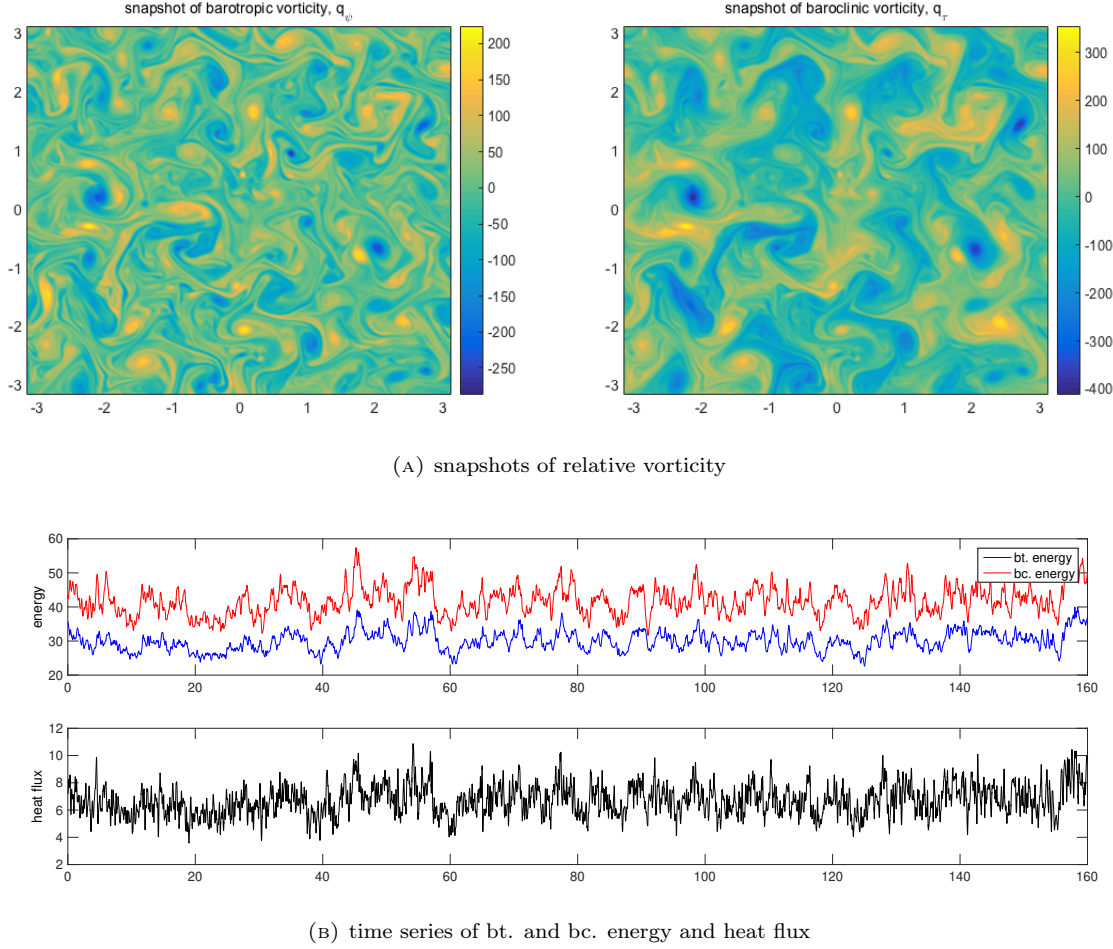


FIGURE 2.1. Snapshots of the unperturbed system in high-latitude ocean regime with no external forcing terms. The barotropic and baroclinic vorticity in steady state are plotted. Homogeneous statistics can be observed in both variables. The following rows show the time-series of the barotropic and baroclinic energy compared with the heat flux representing the meridional heat transfer. Note the strong correlation between the barotropic and baroclinic mode through the snapshots and time-series.

Substitute this into the original disturbance equations (2.1), and focus on the linear part ignoring the Jacobians for quadratic interactions. The linearized system with dissipation terms becomes

$$(3.1) \quad ik_1 A \begin{bmatrix} \hat{\psi}_{\mathbf{k}} \\ \hat{\tau}_{\mathbf{k}} \end{bmatrix} = (-\kappa D - \nu H) \begin{bmatrix} \hat{\psi}_{\mathbf{k}} \\ \hat{\tau}_{\mathbf{k}} \end{bmatrix},$$

with the linearized coefficient matrix from mean shear flow and β -effect

$$A = \begin{bmatrix} (c|\mathbf{k}|^2 + \beta) & -U|\mathbf{k}|^2 \\ U(-|\mathbf{k}|^2 + k_d^2) & c(|\mathbf{k}|^2 + k_d^2) + \beta - \xi U |\mathbf{k}|^2 \end{bmatrix},$$

and the linear terms for dissipation

$$D = \begin{bmatrix} (1-\delta)|\mathbf{k}|^2 & -\sqrt{\delta(1-\delta)}|\mathbf{k}|^2 \\ -\sqrt{\delta(1-\delta)}|\mathbf{k}|^2 & \delta|\mathbf{k}|^2 \end{bmatrix}, \quad H = \begin{bmatrix} |\mathbf{k}|^{2s}|\mathbf{k}|^2 & \\ |\mathbf{k}|^{2s}(|\mathbf{k}|^2 + k_d^2) & \end{bmatrix}.$$

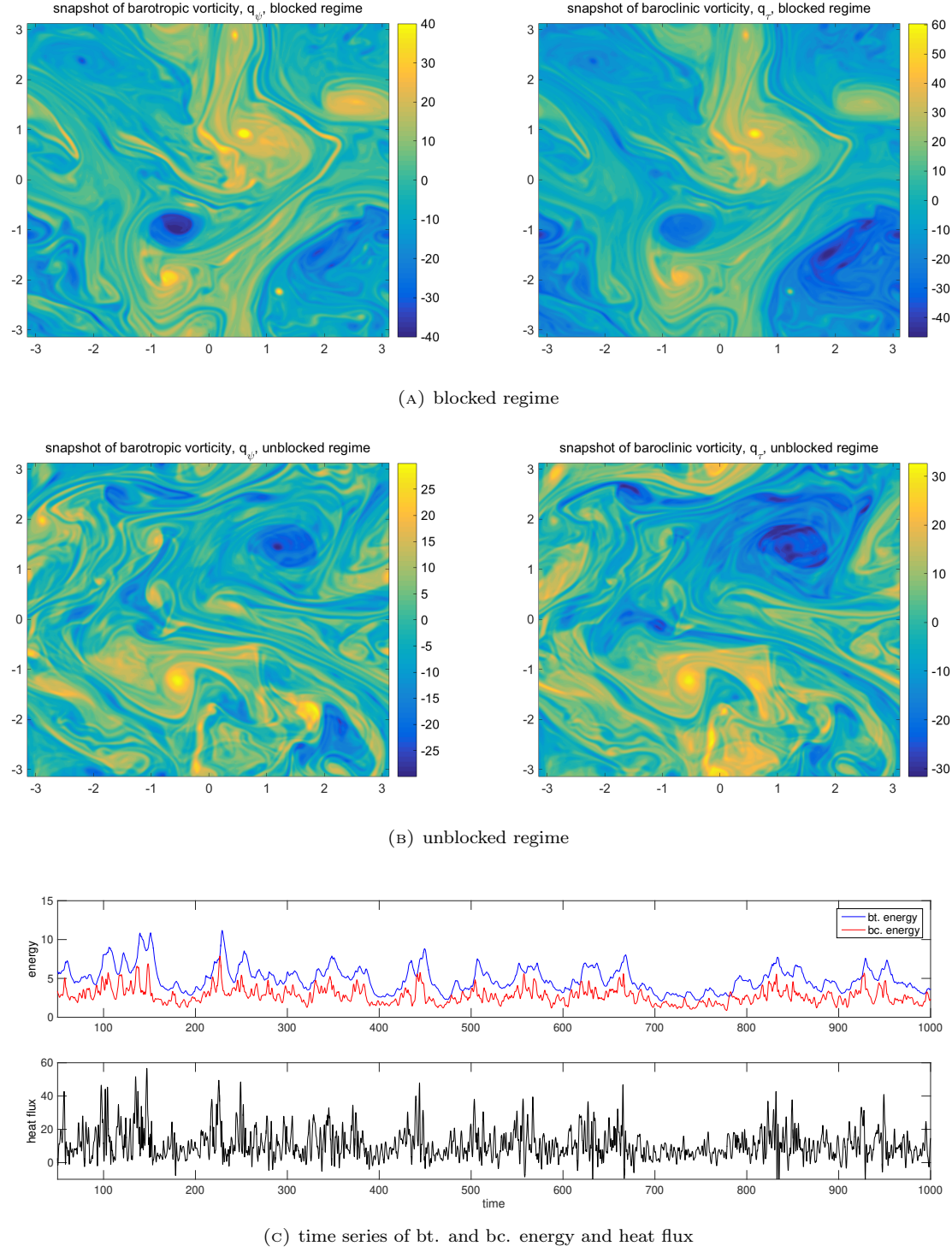


FIGURE 2.2. Snapshots of the unperturbed system in high-latitude atmosphere regime with no external forcing terms. first row: the barotropic and baroclinic vorticity in blocked regime; second row: the barotropic and baroclinic vorticity in unblocked regime. The following rows show the time-series of the barotropic and baroclinic energy compared with the heat flux representing the meridional heat transfer.

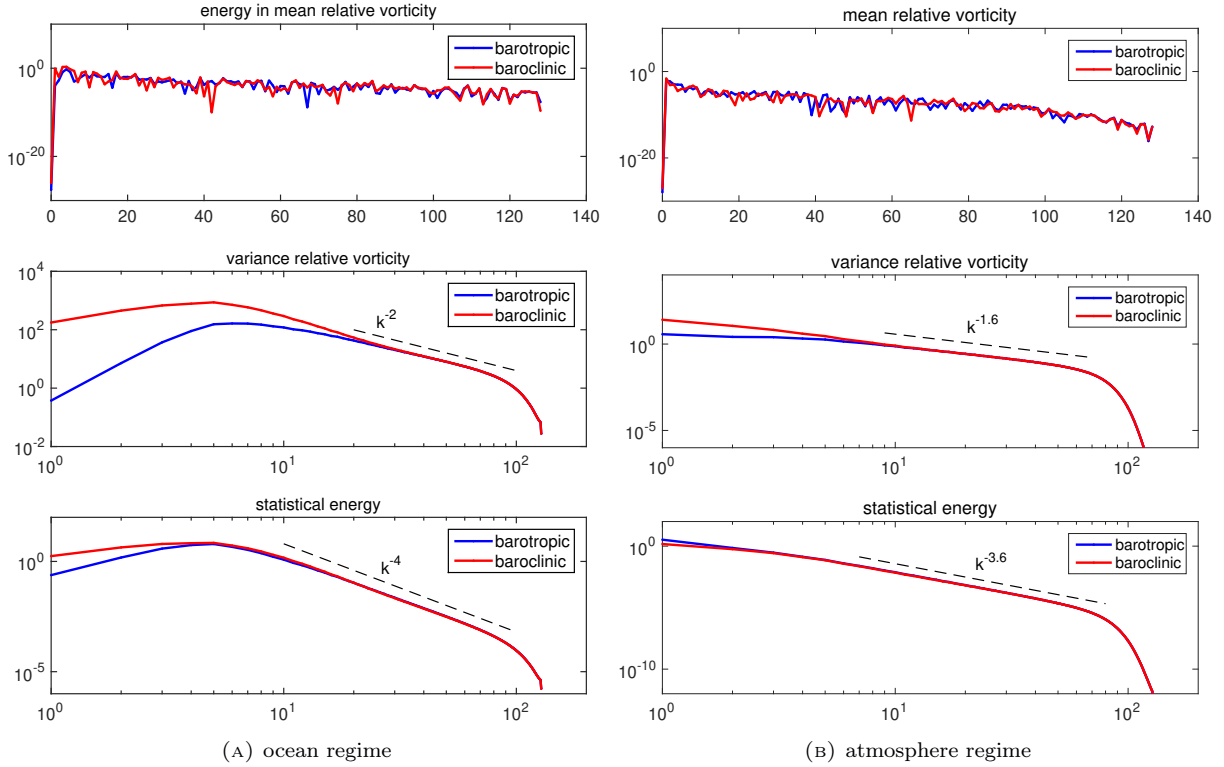


FIGURE 2.3. Time-averaged statistics (in radial average) in mean and second-order moments. The first row compares the statistical mean states, as implied from the homogeneous statistics, the mean states stay in small values within fluctuation errors in both ocean and atmosphere regimes. The following two rows show the variances, $\overline{|q_{\psi,k}|^2}$, $\overline{|q_{\tau,k}|^2}$, and statistical energy, $|k|^2 \overline{|\psi_k|^2}$, $(|k|^2 + k_d^2) \overline{|\tau_k|^2}$, in barotropic and baroclinic modes. Most of the energy and variances are contained in the first 20 modes in both barotropic and baroclinic component in the ocean regime, while in the atmosphere regime the first mode contains most energy of the system.

Now first focus on the instability due to the linear part A and ignore the effects from dissipation. Non-trivial solution $(\hat{\psi}_k, \hat{\tau}_k)$ requires degenerate matrix, $\det A = 0$, that is,

$$(c|\mathbf{k}|^2 + \beta) [c(|\mathbf{k}|^2 + k_d^2) + \beta - \xi U |\mathbf{k}|^2] + U^2 |\mathbf{k}|^2 (-|\mathbf{k}|^2 + k_d^2) = 0.$$

Linear instability takes place in the modes where the imaginary part of the phase speed c becomes positive. Without consideration about the dissipations, the above equation is simply quadratic with real coefficients. For simplicity in calculation, we only consider the equal layer depth case, $\xi = 0$. When the phase velocity has imaginary component, it must take the form

$$(3.2) \quad i\Im c = \frac{\beta k_d^2}{2|\mathbf{k}|^2 (|\mathbf{k}|^2 + k_d^2)} \left(1 - \frac{4U^2}{\beta^2} |\mathbf{k}|^4 \left(1 - |\mathbf{k}|^4/k_d^4 \right) \right)^{1/2}.$$

From (3.2) above, it can first imply that for system with equal layers, (linear) instability can only take place at wavenumbers at

$$(3.3) \quad \frac{\beta}{2U} \leq |\mathbf{k}|^2 \leq k_d^2.$$

So instabilities can only take place at limited wavenumbers.

To measure the linear unstable modes more precisely, we calculate the amplification rate $\Im c$ from (3.2) through numerical computations. Two typical dynamical regimes will be considered here as in the high-latitude ocean and

atmosphere regimes. We choose the shear U_1, U_2 so that both atmosphere and ocean regimes exhibit instability. Note that the ocean regime becomes quite a stiff problem due to the large deformation wavenumber. From the growth rate formula (3.2), it can be observed that in this case with no dissipation effect included, the instability modes are isotropic with constant radius wavenumber $|\mathbf{k}| = \sqrt{k_1^2 + k_2^2}$. Thus we need only consider the zonal wavenumber k_1 and set $k_2 = 0$ for simplicity.

3.2. Nonlinear stability due to quadratic interactions. Through the linear analysis from (3.1), linear instability could occur among a specific range of wavenumbers and energy will increase among the unstable modes. Then it is useful to check the energy mechanism in the nonlinear interactions through the energy conserving quadratic interactions

$$B_{\mathbf{k}}(\mathbf{p}_{\mathbf{k}}, \mathbf{p}_{\mathbf{k}}) = \begin{pmatrix} \sum_{\mathbf{m}+\mathbf{n}=\mathbf{k}} \mathbf{m}^\perp \cdot \mathbf{n} \left(\frac{|\mathbf{n}|}{|\mathbf{m}|} p_{\psi,\mathbf{m}} p_{\psi,\mathbf{n}} + \sqrt{\frac{|\mathbf{n}|^2 + k_d^2}{|\mathbf{m}|^2 + k_d^2}} p_{\tau,\mathbf{m}} p_{\tau,\mathbf{n}} \right) \\ \sum_{\mathbf{m}+\mathbf{n}=\mathbf{k}} \mathbf{m}^\perp \cdot \mathbf{n} \left(\frac{\sqrt{|\mathbf{n}|^2 + k_d^2}}{|\mathbf{m}|} p_{\psi,\mathbf{m}} p_{\tau,\mathbf{n}} + \frac{|\mathbf{n}|}{\sqrt{|\mathbf{m}|^2 + k_d^2}} p_{\tau,\mathbf{m}} p_{\psi,\mathbf{n}} \right) \end{pmatrix}.$$

We can define the nonlinear flux term through the quadratic interactions as

$$(3.4) \quad Q_{F,\mathbf{k}} = \overline{\mathbf{p}_{\mathbf{k}} \cdot B_{\mathbf{k}}(\mathbf{p}_{\mathbf{k}}, \mathbf{p}_{\mathbf{k}})}.$$

Above the overbar can be viewed as the ensemble average, and thus $Q_{F,\mathbf{k}}$ characterizes the nonlinear energy transfer in each wavenumber \mathbf{k} . The negative eigenvalues in Q_F represent the stabilizing effects that dissipate (transfer) the additional energy due to linear instability, while the positive eigenvalues show the additional energy that inject into the linear stable modes.

In Figure 3.1 and 3.2, we compare the results from linear analysis with damping effects and the eigenvalues from the nonlinear flux in both ocean and atmosphere regime. In both regimes we can observe that the most unstable linear modes take place in zonal direction (with $k_y = 0$) and all the meridional modes ($k_x = 0$) become stable due to the damping effects. Correspondingly, the nonlinear flux Q_F has negative eigenvalues in the zonal modes (meaning outflow of energy due to nonlinear interactions) and positive eigenvalues in the meridional modes (meaning inflow of energy). Comparing the ocean and atmosphere regime, it is also important to notice that the ocean regime contains a wider range of unstable modes with larger amplitude due to the relative large deformation frequency k_d , while in the atmosphere regime the strongest nonlinear energy transfers take place at $|\mathbf{k}| = 1$. As we can see in the numerical simulations in the atmosphere regime, this creates a dominant mode with large energy in the spectra at $|\mathbf{k}| = 1$.

Linear stability analysis for zero dissipation and changing layer depth ratio δ are displayed in both atmosphere and ocean regime in Figure 3.3 and 3.4. The growth rates in zonal wavenumber from (3.2) with several two-layer depth ratios δ are compared in the first row. The second row compares the maximum growth rate with changing $0 < \delta < 1$. And the first and last zonal wavenumber that instability begins and ends as well as the wavenumber that maximum growth rate is reached as a function of δ are compared with and without damping effect κ . In the case with no dissipation, there exist an explicit band of wavenumbers with first and last mode when the linear instability takes place. The first two large-scale modes begin with stable, and then instability happens, and there is also an upper bound for the unstable wavenumber. It can also be observed that the ocean regime has a broader unstable band compared with the atmosphere regime, while the growth rates of the unstable modes in the ocean regime are weaker compared with the atmosphere case. Also the unstable band changes when the layer depth ratio δ varies. There exists an low bound ratio δ_{\min} for instability to take place. The atmosphere regime gets a relatively larger δ_{\min} compared with the ocean regime where instability happens at small δ . Finally it can be observed that the maximum growth rate first increases and then decreases as we increase the value of the depth ratio δ .

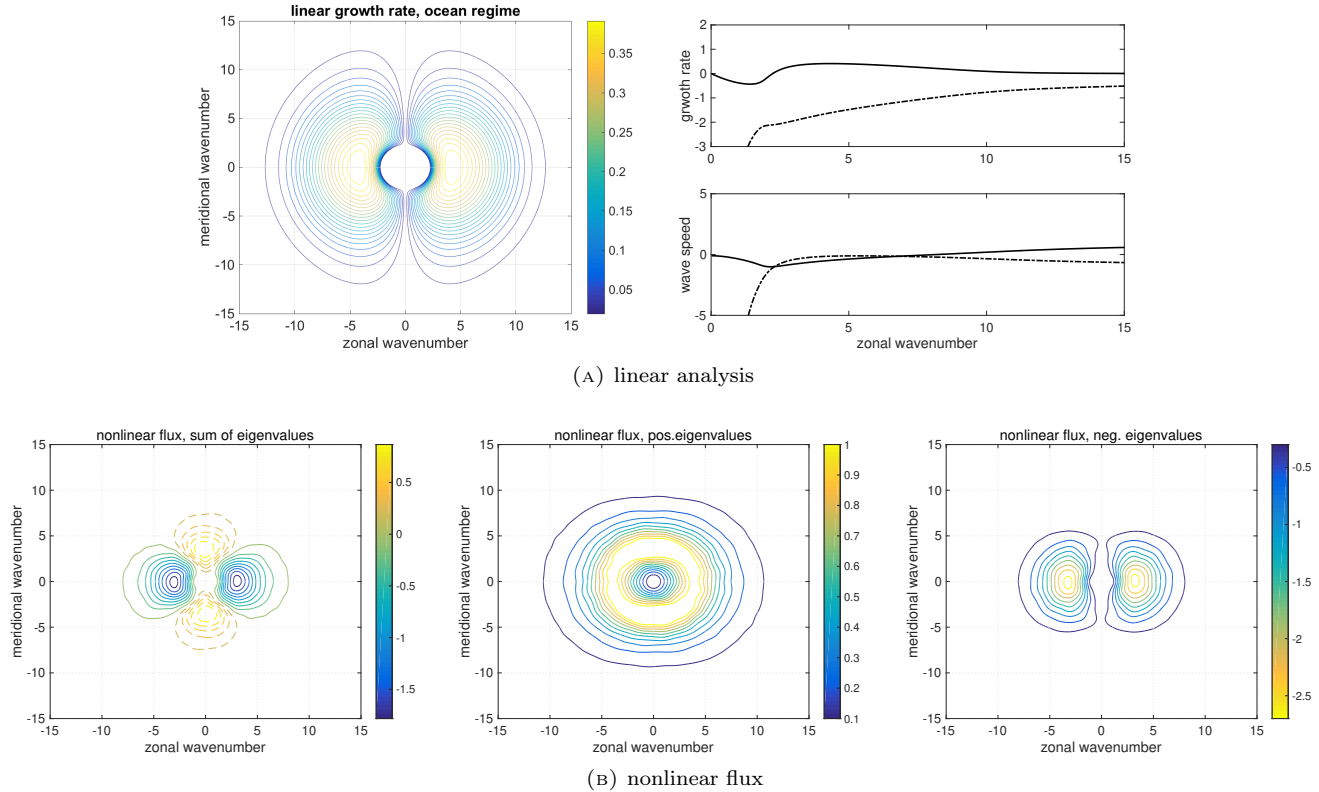


FIGURE 3.1. Stability analysis from linear analysis and nonlinear flux in ocean regime using parameters in Table 2. The first row is the linear growth rate with damping effects included. Also the zonal wave speed and growth rate are compared for two branches in the solution. The second row shows the eigenvalues of the nonlinear flux Q_F in each wavenumber in the two-dimensional domain. The unstable direction, stable direction, together with the total instability (that is, the trace of the blocked-matrix $\text{tr}Q_F$ for each wavenumber) are all plotted. It can be noticed that the strongest damping modes are zonal modes, $k_y = 0$, while the negative eigenvalues are radial symmetric. Correspondence can be observed compared the linear and nonlinear results. In the test model, the deformation frequency is set as $k_d = 10$. All the unstable modes are with in $|\mathbf{k}| < k_d$.

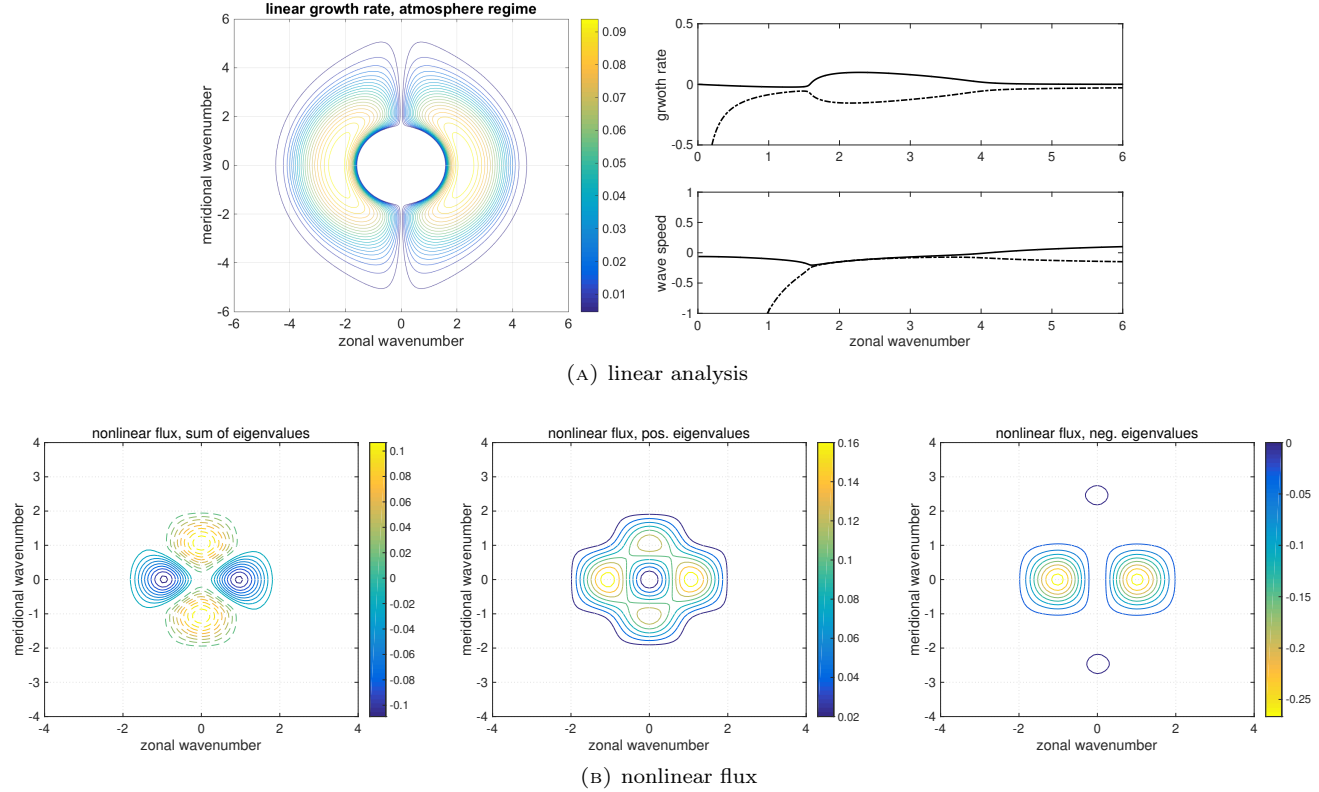


FIGURE 3.2. Stability analysis from linear analysis and nonlinear flux in atmosphere regime using parameters in Table 2. The first row is the linear growth rate with damping effects included. Also the zonal wave speed and growth rate are compared for two branches in the solution. The second row shows the eigenvalues of the nonlinear flux Q_F in each wavenumber in the two-dimensional domain. The unstable direction, stable direction, together with the total instability (that is, the trace of the blocked-matrix $\text{tr}Q_F$ for each wavenumber) are all plotted. It can be noticed that the strongest damping modes are zonal modes, $k_y = 0$, while the negative eigenvalues are radial symmetric. Correspondence can be observed compared the linear and nonlinear results. In the test model, the deformation frequency is set as $k_d = 4$. All the unstable modes are with in $|\mathbf{k}| < k_d$.

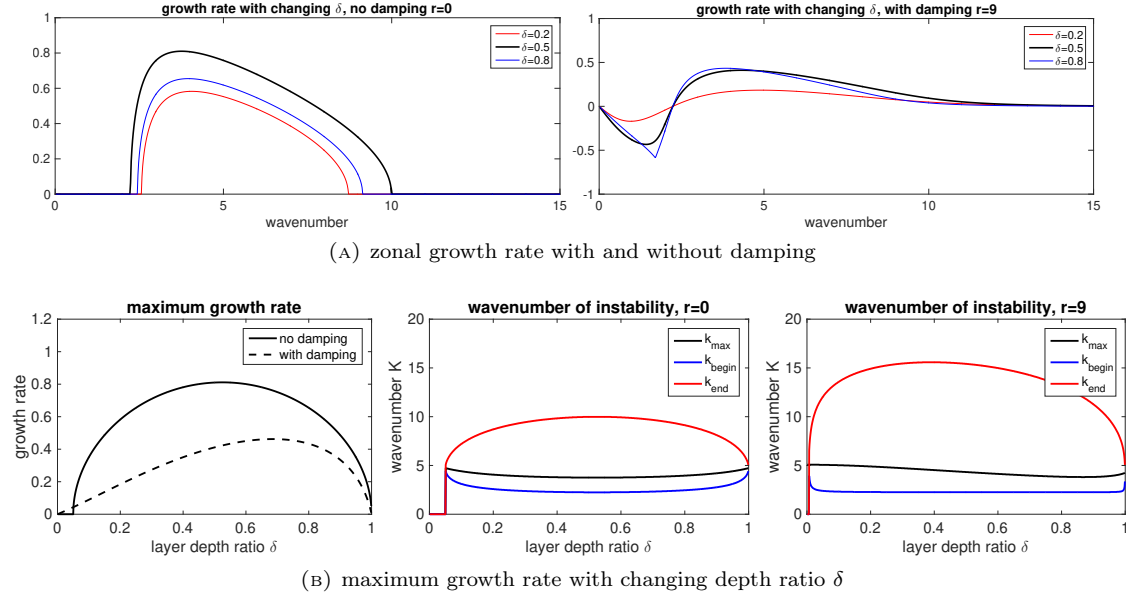


FIGURE 3.3. The effects from the layer depth ratio δ in the ocean regime with and without damping effect κ . The first row shows the zonal growth rates with several depth ratio $\delta = 0.2, 0.5, 0.8$. The second row displays the maximum growth rates with changing depth ratio δ as well as the wavenumber at first, last and largest instability.

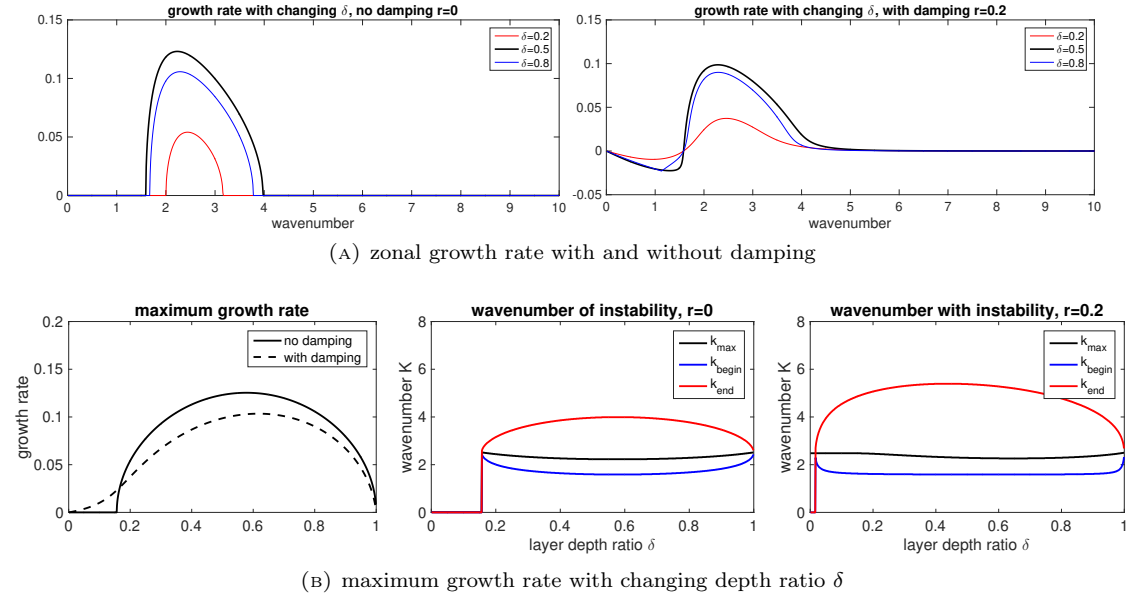


FIGURE 3.4. The effects from the layer depth ratio δ in the atmosphere regime with and without damping effect κ . The first row shows the zonal growth rates with several depth ratio $\delta = 0.2, 0.5, 0.8$. The second row displays the maximum growth rates with changing depth ratio δ as well as the wavenumber at first, last and largest instability.